BULLETIN OF THE POLISH ACADEMY OF SCIENCES
TECHNICAL SCIENCES, Vol. 67, No. 4, 2019
DOI: 10.24425/bpasts.2019.130180

Anisotropy of mechanical and structural properties in AA 6060 aluminum alloy following hydrostatic extrusion process

S. PRZYBYSZ[1]*, M. KULCZYK[1], W. PACHLA[1], J. SKIBA[1], M. WRÓBLEWSKA[1], J. MIZERA[2], and D. MOSZCZYŃSKA[2]

[1] Institute of High Pressure Physics of the Polish Academy of Sciences UNIPRESS, Sokołowska 29/37, 01-142 Warsaw, Poland
[2] Warsaw University of Technology, Faculty of Materials Science and Engineering, Wołoska 141, 02-507 Warsaw, Poland

Abstract. The study attempts to investigate the influence of severe plastic deformation (SPD in the hydrostatic extrusion (HE) process on the anisotropy of the structure and mechanical properties of the AA 6060 alloy. Material in isotropic condition was subjected to a single round of hydrostatic extrusion with three different degrees of deformation ($\varepsilon = 1.23, 1.57, 2.28$). They allowed the grain size to be fragmented to the nanocrystalline level. Mechanical properties of the AA 6060 alloy, examined on mini-samples, showed an increase in ultimate tensile strength (UTS) and yield strength (YS) as compared to the initial material. Significant strengthening of the material results from high grain refinement in transverse section, from ~220 μm in the initial material to ~300 nm following the HE process. The material was characterized by the occurrence of structure anisotropy, which may determine the potential use of the material. Static tensile tests of mini-samples showed ~10% anisotropy of properties between longitudinal and transverse cross-sections. In the AA6060 alloy, impact anisotropy was found depending on the direction of its testing. Higher impact toughness was observed in the cross-section parallel to the HE direction. The results obtained allow to analyze the characteristic structure created during the HE process and result in more efficient use of the AA 6060 alloy in applications.

Key words: hydrostatic extrusion, anisotropy, mechanical properties, grain refinement.

1. Introduction

Aluminum alloys of the 6XXX series (Al-Mg-Si) are among the most popular alloys to be applied in light industrial constructions. They are characterized by a good strength-to-density ratio as well as high formability. The alloys have sound corrosion resistance, weldability and good susceptibility to plastic processing. With their properties, they can be used in construction as well as the automotive and aerospace industry, and wherever the material requires high strength while maintaining relatively low weight. Among others, supporting elements for buses, ships and bridges are made of them [1, 2].

Aluminum alloys are often plastic-processed using SPD methods due to their high plasticity to improve mechanical properties and increase the strength-to-weight ratio. Severe plastic deformation can be generated using a number of methods described in the literature, for example: equal-channel angular extrusion (ECAP) [3, 4], high pressure torsion (HPT) [5, 6], accumulative roll-bonding (ARB) [7, 8], cyclic extrusion compression (CEC) [9, 10] or hydrostatic extrusion (HE) [11, 12]. Material properties after such processes depend strongly on the degree of microstructure refinement. According to the Hall-Petch equation [13, 14] grain refinement leads to the increase of material strength according to the mechanism of strengthening by grain boundaries [15].

The efficiency of breaking the grain using the HE method has been demonstrated for many metals and alloys. Ultra-fine grain (UFG) or nanocrystalline (NC) structures were obtained, among others in aluminum and its alloys [16, 17], copper and its alloys [18–20], titanium [21, 22], austenitic steel [23, 24], nickel [25, 26] and many other materials. The use of the HE method leads to creating a characteristic microstructure in the deformed material. In materials such as titanium CP Ti grade 2 [21], CP Ti grade 3 [27], austenitic steel 316L [23, 24] or the CuCrZr copper alloy [28], after HE the texture with grains elongated in the direction of extrusion was observed in the longitudinal cross-section, whereas in the transverse direction these grains are visible as equiaxial ones. This results in anisotropy of mechanical properties of the material after the deformation process in mutually perpendicular directions. A detailed description of this phenomenon is presented in [27] for CP Ti grade 3 after HE. The yield strength in accordance with the extrusion direction was YS = 915 MPa, and in the perpendicular direction YS = 560 MPa. Such anisotropy has a significant impact on the use of the material, e.g. for titanium, this excludes the use for long orthopedic implants operating under complex stress conditions [22]. A positive effect of structure anisotropy was demonstrated in the CuCrZr alloy, where electrodes for the spot welding process made of the material with strong anisotropy after HE showed a significantly higher lifetime as compared to the material obtained from the combination of ECAP and HE processes and characterized by similar mechanical properties and a structure close to the isotropic one [28].

Plastic anisotropy of materials can be calculated from the tensile test data by two methods: by analyzing the strain ratio

*e-mail: sylwia@unipress.waw.pl

Manuscript submitted 2018-11-20, revised 2019-01-18, initially accepted for publication 2019-02-19, published in August 2019

vs elongation relationship, or by relating partial strains due to width and thickness strains to the total elongation. It has been shown that the first method makes it possible to determine precisely the value which constitutes the anisotropy coefficient with well-defined physical meaning [29].

The effect of structural anisotropy, apart from its influence on static mechanical properties, also exerts a strong influence on dynamic properties. The loads applied to mechanical systems (machines and their components, construction structures, etc.) are often dynamic in nature. Different materials exhibiting similar strength properties under a static load may exhibit a different ability to carry dynamic loads under a dynamic load.

Surveys of anisotropy following SPD processes, especially the HE process, are rarely found in professional literature. Literature includes data e.g. for the AA 7075 aluminum alloy following the cold rolling process for which the impact toughness and its anisotropy were tested, higher for the direction of rolling [30]. In contrast to materials reinforced by means of conventional methods, materials subjected to SPD processes with a finely divided microstructure sometimes exhibit an abnormal increase in impact toughness along with increased strength. For the AA 7075 alloy, after cryo-rolling, the increase in impact toughness with increasing the deformation was found. After a 70% plastic deformation, the impact energy increased by ~60% [31]. A similar effect was observed in the Al-Cu alloy following the ECAP process, in which, with the increase of plastic deformation, the increase in impact toughness occurred with the simultaneous increase in mechanical properties [32].

The study presents the influence of the plastic deformation level generated by the HE method on the anisotropic character of structural and mechanical changes in the AA 6060 alloy. The influence of structural anisotropy on mechanical properties and impact toughness measured depending on the test direction was described. Studies will allow for better understanding of the characteristic microstructure created in the HE process and its impact on mechanical properties of rods extruded from the AA 6060 alloy.

2. Experimental phase

The aluminum AA 6060 alloy, supplied in the form of bars with the diameter of 50 mm, in T4 condition (supersaturated and naturally aged), was used for tests. T4 condition corresponds to heating the material up to 540°C in a salt bath for 15 minutes, then tempering in water and storing at room temperature for a long time. This procedure ensures that the main Mg and Si alloy elements are present in the alloy in the form of a solid solution and separation particles of Mg_2Si and Mg_5Si_6 are not formed as a result of natural aging [33, 34]. The chemical composition of the alloy based on the PN-EN 573–3 standard is presented in Table 1. The material structure in the initial condition and following plastic deformation was characterized based on the following parameters: the average equivalent diameter of the grain d_{eq} (defined as the diameter of the circle which has the surface equal to the surface of the given grain), the coefficient of variation $CV(d_{eq})$, defined as the ratio of standard deviation

Table 1
Chemical composition of AA 6060 alloy in wt%

Content of elements, wt%								
Mg	Si	Fe	Zn	Cu	Mn	Ti	Cr	Al
0.35–0.6	0.3–0.6	0.1–0.3	0.15	0.1	0.1	0.1	0.05	rest

of the diameter to d_{eq}, and the coefficient of grain elongation α, determined as the ratio of the average maximum grain diameter to d_{eq}. Sizes and shapes of grains before and after the HE process were determined using the image analysis method with MicroMeter software [35]. These parameters were determined in over 100 randomly selected grains in the transverse (perpendicular to the rod axis, TD) and longitudinal (parallel to the rod axis, LD) cross-sections. Microstructural observations for the initial material were carried out using the Nikon Eclipse LV150 optical microscope and after plastic deformation these were carried out using the FEI TECNAI G2 F20 transmission electron microscope. In both cases, TD and LD rod cross-sections were studied.

The microstructure of the AA 6060 alloy in the initial condition is shown in Fig. 1. Both in the TD and LD cross-sections,

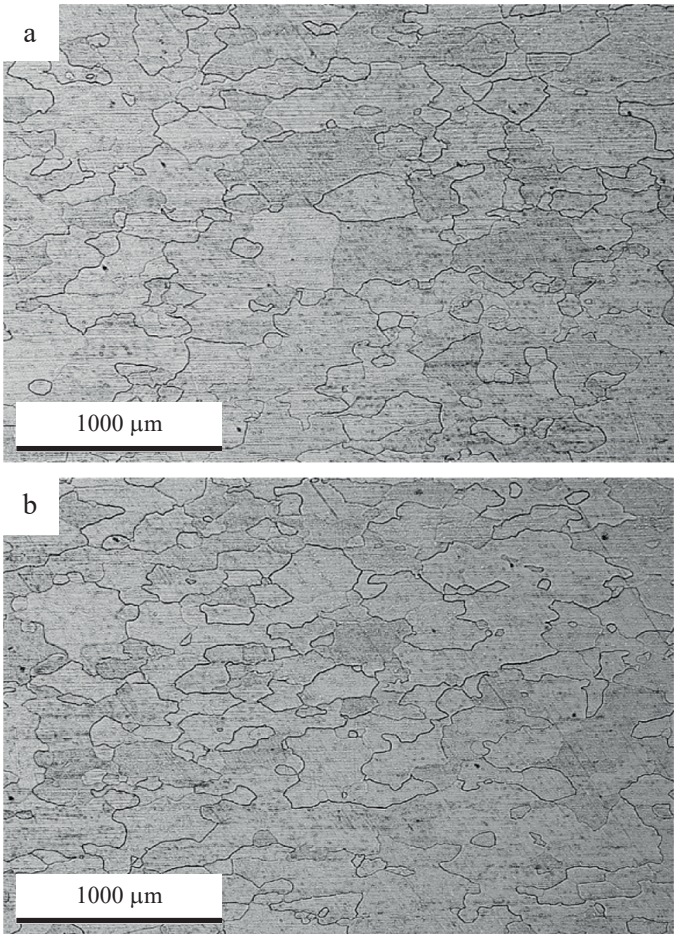

Fig. 1. Microstructure of the AA 6060 initial material: a) TD cross section, b) LD cross-section

the value of the average equivalent diameter d_{eq} was ~220 μm, and of standard deviation SD(d_{eq}) ~90 μm. The average coefficient of grain elongation for both cross-sections was $\alpha \sim 1.5$. Similar α coefficients and the d_{eq} value for both cross-sections evidence a structure similar in nature to the isotropic condition. The structural isotropy of the material in the initial condition is important for the analysis of the influence of deformations on structural changes in the direction parallel and on those perpendicular to the extrusion direction.

AA 6060 alloy rods with diameters of 50 mm and 35 mm were subjected to a single round of hydrostatic extrusion with deformations presented in Table 2. The methodology of the HE process has been described, among others in [36–37]. The amount of the deformation in the HE process is described by the reduction ratio R or true deformation ε. The reduction ratio R is the ratio of transverse cross-sections before and after the extrusion. The true strain ε expresses the natural logarithm of the reduction ratio, $\varepsilon = \ln R$, and the percentage deformation is calculated according to the following relationship: $r\% = \left(1 - R^{-1}\right)\ 100\%$.

Table 2
Amount of plastic deformations in hydrostatic extrusion process of AA 6060 alloy

Condition	Reduction grade R	True deformation ε	Percentage deformation $r\%$
Initial	1	0	0
ϕ50 → ϕ27 mm	3.43	1.23	71
ϕ35 → ϕ16 mm	4.79	1.57	79
ϕ50 → ϕ16 mm	9.77	2.28	90

Hydrostatic extrusion was carried out as a single operation on UNIPRESS presses designed and made at the Institute of High Pressure Physics of the Polish Academy of Sciences working in the working pressure range of up to 1.4 GPa, through the die with top angle $2\alpha = 45^{o}$ at room temperature, for final diameters of 16 mm or 27 mm, as listed in Table 2. To minimize the adiabatic heating effect during the severe plastic deformation, rods at the exit from the die were cooled intensively with running cold water. The adiabatic heating effect is significant especially in the HE process characterized by high deformation speeds under high pressure conditions. The amount of the adiabatic heating effect ΔT during the HE process is proportional to the extrusion pressure p and can be estimated according to the following relationship [38, 39]:

$$\Delta T = \beta\left(\frac{p}{\rho c}\right) \tag{1}$$

where p is the extrusion pressure, ρ and c stand for the density and specific heat of the material, and β marks what part of the extrusion mechanical work is converted into heat. For the HE process, it can be assumed that the β parameter is ~0.95, which results from high extrusion speed and good insulating conditions of the lubricating layer [24].

The microhardness measurements were carried out using the automated Zwick-Roell ZHV1-A hardness tester with a load of 200 g for 15 s. Static tensile tests in both TD and LD cross-sections of extruded rods were measured on the five mini-samples with the width of 0.8 mm, the thickness of 0.6 mm and the length of the measuring part of 5 mm using the ZWICK 780 machine. Dynamic impact tensile tests were carried out using the Instron Dynatup 9250HV High Speed Impact Tester. In the TD cross-section, the test was carried out using the Charpy method according to PN-EN ISO 148–1: 2010 with impact energy of 300 J on samples of 10×10 mm with an U-shaped notch having the depth of 5 mm and the bottom rounding radius of 1 mm. In the LD cross-section, the impact tensile test was carried out with impact energy of 500 J on five-fold samples with the geometry and diameter of 8 mm. Both tests were carried out at room temperature with impact speed of 4.7 m s^{-1}. Samples were selected so that their active cross-sections taking active part in the cracking were the same and amounted to 50 mm^2, as presented in Fig. 2.

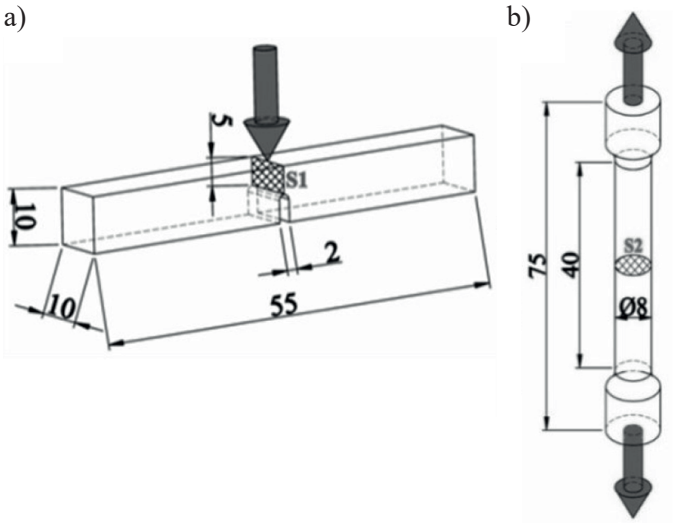

Fig. 2. Diagram and dimensions of samples used in impact toughness test: a) using the Charpy method, b) using the impact tensile method

Tests in the perpendicular direction were marked K_{CH} while tests in the parallel direction were marked K_{IT}.

The deviation of impact toughness after the HE process from the isotropic value for the initial material was calculated according to the following formula:

$$\Delta K_{CH,\,IT} = \left[1 - \frac{K_{INIT(CH,\,IT)}}{K_{CH,\,IT}}\right] 100\% \tag{2}$$

where:

K_{CH} and K_{IT} – impact toughness measured by the Charpy or impact tensile method,

K_{INIT} – impact toughness of the initial material.

Calculated values allowed for the quantitative comparison of impact toughness changes in the transverse and longitudinal cross-sections of the material after the HE process in relation to the isotropic initial material.

Results of mechanical properties measures of the AA 6060 alloy in the initial condition are shown in Table 3.

Table 3
Mechanical properties of initial AA 6060 material

Alloy	UTS (MPa)	YS (MPa)	ε_f (%)	$K_{INIT(CH)}$ (J cm^{-2})	$K_{INIT(IT)}$ (J/cm^{-2})	HV0.2 LD	HV0.2 TD
AA 6060	153	86	26	74	20	54	52

3. Results and discussion

3.1. Hydrostatic extrusion. Pressure characteristics of the HE process for the AA 6060 alloy for the three deformation grades ε used are shown in Fig. 3. Initial pressure rises represent compressibility of the pressure medium, and flattened plateau means stabilizing the HE processes in which the deformation occurs at constant extrusion speed, while pressure drops correspond to the process of expansion of the working chamber. The extrusion pressure of the AA 6060 alloy increases with the increase in the degree of the deformation in the range between 300 and 550 MPa, as presented in Fig. 3. Higher extrusion pressure means more mechanical work of the plastic deformation, which attains higher temperature in the deformation zone of the material in the die (higher adiabatic heating). Assuming for equation (1) values of density $\rho = 2.7$ g cm^{-3} and specific heat $c = 0.898$ J g^{-1} K^{-1} and assuming the value of $\beta = 0.95$ for registered extrusion pressures, for the AA 6060 alloy, the adiabatic heating effect ΔT is in the range of $\sim$115–205°C. This corresponds to the homologous temperature range of $T_h = T/T_m = 0.44$–0.54, where T is the estimated temperature,

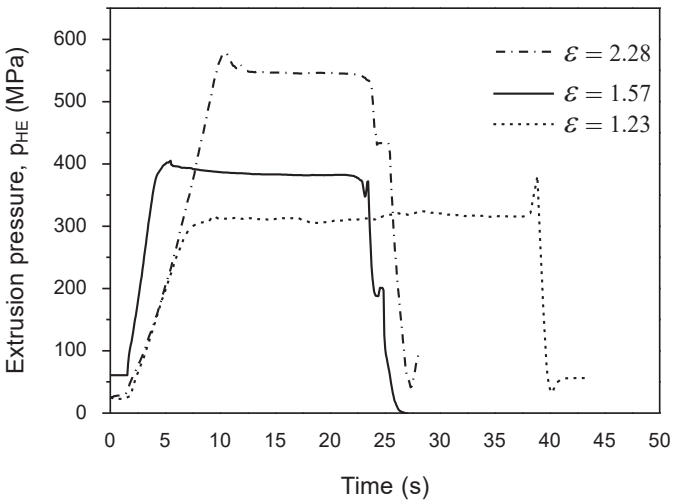

Fig. 3. Pressure characteristics of hydrostatic extrusion for the AA 6060 alloy in three deformation grades

Table 4
Adiabatic heating temperature during hydrostatic extrusion of AA 6060 alloy

ε	ΔT(°C)	$T_h = T/T_m$ [(a)]
1.23	116	0.44
1.57	150	0.48
2.28	203	0.54

[(a)] Melting temperature of AA 6060 $T_m = 610$°C

and T_m is the melting temperature, both in K degrees, as presented in Table 4.

Estimated temperatures indicate that temperature in the deformation zone during the HE process reaches values characteristic for the dynamic recovery processes of the AA 6060 alloy, which weaken the effects of deformation strengthening.

3.2. Structure following hydrostatic extrusion. The effect of the HE process on the structure morphology in the AA 6060 alloy is shown on the example of the highest deformation $\varepsilon = 2.28$, as presented in Fig. 4. There is clear structural

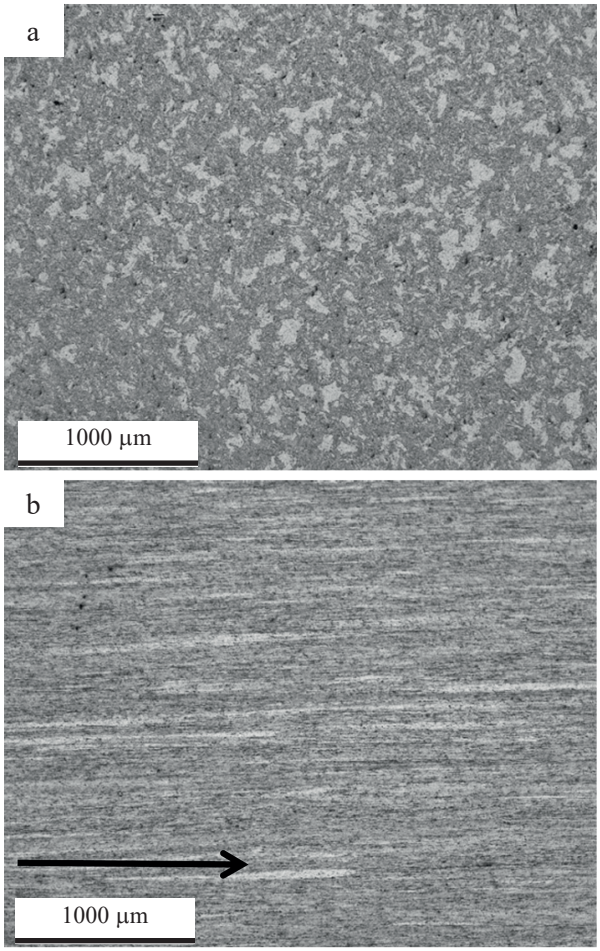

Fig. 4. AA 6060 alloy microstructure after hydrostatic extrusion process with true strain $\varepsilon = 2.28$: a) transverse TD cross-section, b) longitudinal LD cross-section. The arrow indicates the extrusion direction

anisotropy after the HE process. It is characterized by an equiaxed structure in the transverse TD cross-section (Fig. 4a) and the structure with elongated grains, arranged in characteristic bands on the parallel LD cross-section (Fig. 4b). Structure changes for the two remaining deformation grades are similar to those shown in Fig. 4. Meanwhile, Fig. 5 shows TEM images illustrating the effect of plastic deformation on the grain size following the HE process. In the LD cross-sections of bars(Fig. 5b, 5d, 5f), regardless of the deformation grade, a strong morphological texture appears with grains elongated in the extrusion direction. In the TD direction (Fig. 5a, 5c, 5e), these grains are in the majority close to equiaxial. The average

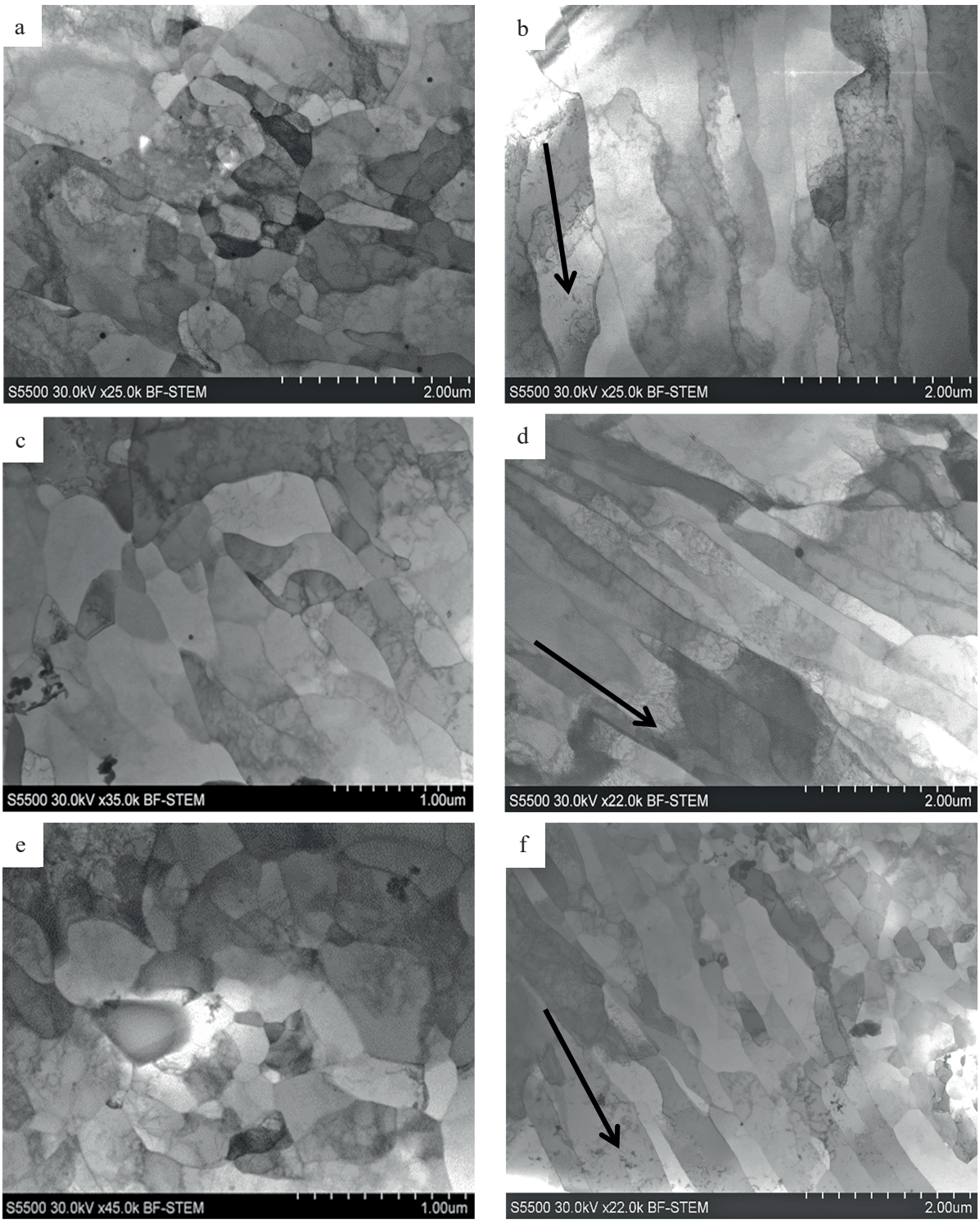

Fig. 5. TEM photos of the AA 6060 alloy after HE process for different values of strain: a, b) $\varepsilon = 1.23$, c, d) $\varepsilon = 1.57$ and e, f) $\varepsilon = 2.28$. Photos (a, c, e) – transverse TD cross-section, photos (b, d, f) – longitudinal LD cross-section. *Note*: arrows indicate the extrusion direction (a)

grain size in the cross-section decreased from 220 μm in the initial material (Fig. 1a) to ∼300 nm after the HE process, as presented in Table 5. For all strain values ε a similar grain size d_{eq} is observed with differences below 8%. Lack of significant differences in grain size is associated with the presence of the significant, adiabatic heating effect observed during the HE process and growing with the deformation, as presented in Table 4. Adiabatic heating counteracts fragmentation of the structure and inhibits and mitigates the effects of strengthening.

Table 5
Average equivalent grain diameter d_{eq}, coefficient of variation $CV(d_{eq})$ and elongation coefficient α in AA 6060 alloy in the initial condition and after the hydrostatic extrusion process

	initial	$\varepsilon = 1.23$	$\varepsilon = 1.57$	$\varepsilon = 2.28$
d_{eq}	217 μm	292 nm	314 nm	291 nm
$CV(d_{eq}) = SD/d_{eq}$	0.42	0.54	0.31	0.51
α_{TD}	1.49	1.56	1.66	1.34
α_{LD}	1.42	1.74	2.07	1.82
α_{LD}/α_{TD}	0.95	1.12	1.25	1.36

The transformation process of the microstructure is better illustrated by measurements of mean angles of grains disorientation before and after the HE process, as presented in Fig. 6. In the non-deformed initial material, the occurrence of high-angle boundaries at the level of nearly 80% is observed. At the lowest deformation grade ($\varepsilon = 1.23$), the dominance of subgrains with an angle of low disorientation below 5° is observed at the level of nearly 60%. For true strain values $\varepsilon = 1.57$ and $\varepsilon = 2.28$, the percentage share of low angle boundaries ($deq < 5°$) decreases with respect to the smallest deformation. For the disorientation angle between 5–15°, the maximum percentage of ∼50% is observed for average deformation $\varepsilon = 1.57$. At the highest deformation ratio, the share in particular ranges of disorientation angles has similar values and is between 30 and 40%. This is the effect of the competitive impact of high plastic deformation and thermally activated dynamic healing processes, as a result of which the structural defects are regrouped and thus a more-developed equiaxial microstructure is formed, as seen in Fig. 5e. In the transverse cross-section, the grains have remained close to equiaxed in nature, especially at the highest deformation ratio, $\alpha_{TD} = 1.34$, as presented in Table 5. In the longitudinal cross-section, the extended structure $\alpha_{LD} = 1.82$ is still visible, as presented in Fig. 5f.

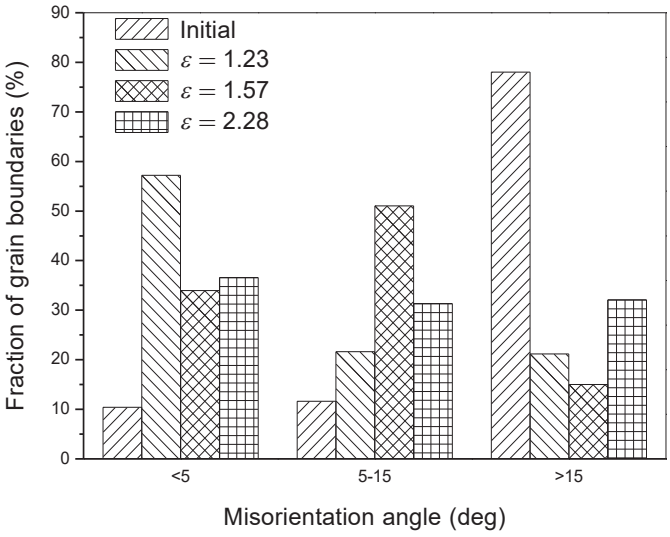

Fig. 6. Grain disorientation angles in AA 6060 alloy in the initial condition and after the hydrostatic extrusion process

Figure 7 shows the ratio of grain elongation in the LD cross-section in relation to grains in the TD cross-section, α_{LD}/α_{TD}. In the initial material, which is characterized by similar grain size in both cross-sections, the ratio is ∼1. With increasing deformation, the difference in grain morphology increases and at the highest deformation α_{LD}/α_{TD} is ∼1.36. The most elongated grains in longitudinal cross-section $\alpha_{LD} = 2.07$ are observed with medium deformation $\varepsilon = 1.57$ (Table 5) for which the share of boundaries with average angles of 5–15° is the highest, at ∼50%, as presented in Fig. 6. For this deformation, adiabatic heating is not effective enough to compensate for grain elongation.

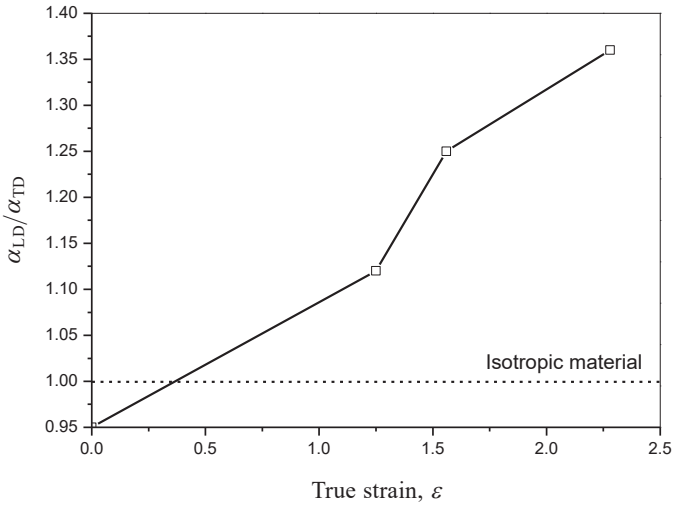

Fig. 7. Grain elongation in longitudinal LD cross-section in relation to grains from transverse TD cross-section for AA 6060 alloy after the hydrostatic extrusion process

3.3. Mechanical properties. The anisotropy of mechanical properties for the AA 6060 alloy is illustrated by the results of strength measurements made on mini-samples in two perpendicular directions, as seen in Fig. 8. The nature of changes in ultimate tensile strength (UTS) and yield strength (YS) properties is similar, and higher values are obtained for the longitudinal direction. Taking account of the results in Fig. 8, it can be seen that the anisotropy of mechanical properties is considerably more strongly influenced by the grain elongation ratio in the direction longitudinal to the transverse α_{LD}/α_{TD} than the absolute grain elongation in the deformation (extrusion) direc-

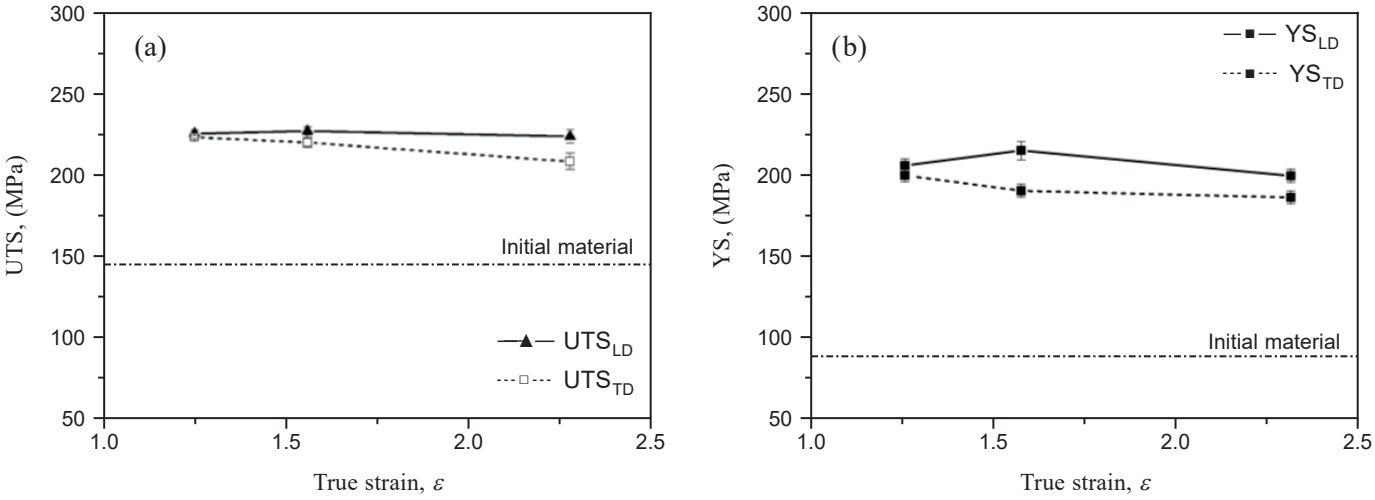

Fig. 8. Mechanical properties as a function of true strain from transverse TD and longitudinal LD cross-sections for AA 6060 alloy after the hydrostatic extrusion process: (a) UTS – ultimate tensile strength, and (b) YS – yield stress

tion α_{LD}, and the UTS and YS values measured indicate ~10% anisotropy with higher values in the longitudinal direction.

3.4. Hardness. The nature of microhardness changes HV0.2 with the deformation change is shown in Fig. 9. As one can observe, there is no hardness anisotropy in the AA 6060 alloy. Average microhardness reaches a maximum value of ~90HV0.2 for the lowest deformation, which is an increase of almost 70% as compared to the initial material. It is associated with the highest density of accumulated defects in the material that have not been effectively cured by the lowest thermal effect. For a higher deformations ratio, the thermal effect is more effective in lowering hardness. It is noticeable that the structural homogeneity of the material after the HE process is increased, which is indicated by the decrease in the hardness change coefficient CV(HV0.2). The homogenization of the structure, and hence the hardness, is small in comparison

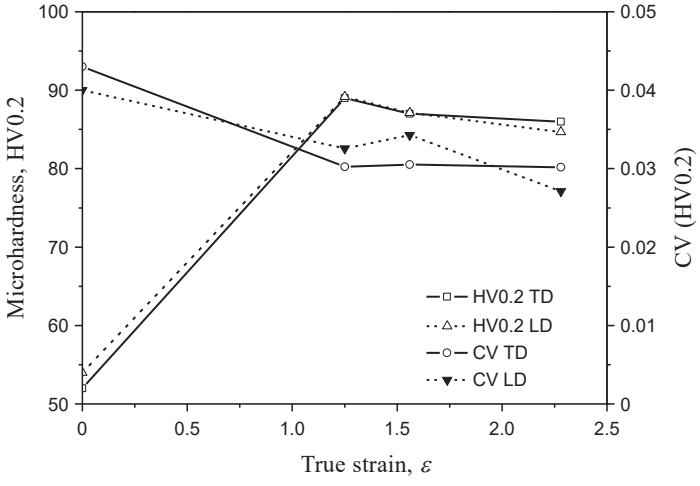

Fig. 9. Microhardness in transverse and longitudinal cross-sections of the AA 6060 alloy, in the initial condition and after the hydrostatic extrusion process

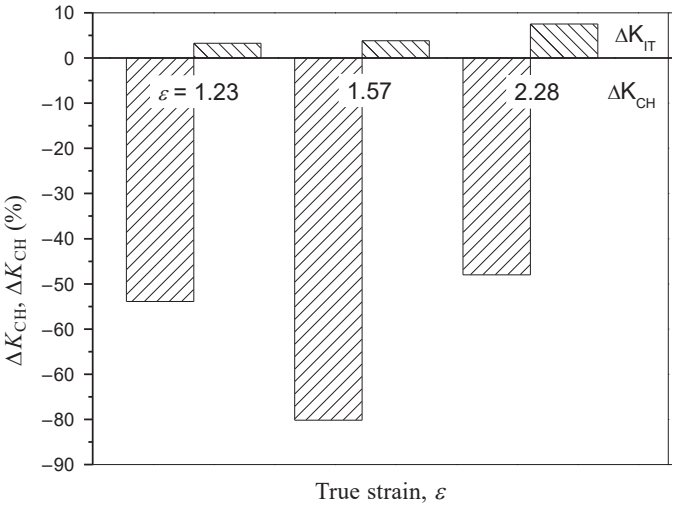

Fig. 10. Impact toughness variations for AA 6060 alloy after the HE process in transverse K_{CH} and longitudinal K_{IT} cross-sections with respect to the isotropic initial material K_{INIT} as the function of true strain ε

with the initial material (~25%), yet clear and associated with higher thermal effects.

3.5. Impact toughness. The deviation from the impact toughness isotropy in the AA 6060 alloy as a function of deformation in the HE process is shown in Fig. 10. Strong impact toughness anisotropy of extruded rods is observed. The AA 6060 alloy shows significantly lower resistance to dynamic loads in the direction perpendicular to the extrusion direction ΔK_{CH}. The greatest decrease of impact toughness as compared to the initial material, at as much as 80%, was observed with the medium true strain $\varepsilon = 1.57$. Increasing the true strain to $\varepsilon = 2.28$ leads to a drop in impact toughness by ~50%. The change of the direction of application of the dynamic force parallelly to the extrusion direction leads, regardless of the deformation ratio, to a slight increase

in impact toughness ΔK_{IT}, reaching the maximum value below 10% for the highest true strain $\varepsilon = 2.28$, as seen in Fig. 10. Thus, it can be seen that for the highest plastic deformation of the AA 6060 alloy using the HE method, the dynamic impact toughness scale $\Delta K_{IT} \sim 8\%$, as seen in Fig. 10. As noted above, a similar effect of impact toughness increase along with the strength was observed in the Al-Cu alloy after the ECAP process [32].

Impact toughness results reflect changes in the structure and in the static strength of the AA 6060 alloy. The greatest decrease in transverse impact toughness K_{CH} after an average deformation grade ($\varepsilon = 1.57$) corresponds to the strongest grain elongation in the extrusion direction α_{LD} (Table 5), i.e. the strongest microstructure texturing after the HE process. The increase in deformation due to the stronger thermal effect accompanying it during the deformation and the stronger healing effects associated with it (Fig. 5e, 5f) lead to the formation of a more ordered and equiaxial microstructure in both cross-sections (lower transverse α_{TD} and longitudinal α_{LD} extensions, Table 5). This in turn inhibits the decrease in impact toughness while reducing the hardness and static mechanical properties measured independently of the test direction. The increase in longitudinal impact toughness K_{IT} at the level of $\sim$10% indicates that the force applied dynamically along the elongated grains interacting with the cross-section with an average size of equiaxis grains $\sim$300 nm (Fig. 5a, 5c, 5e) induces the behavior of the material as UFG with a large proportion of grain boundaries, which leads to an increase in impact toughness while at the same time increasing strength. Otherwise, with the force applied dynamically transversely to the extrusion direction, it affects the cross-section with larger surfaces of elongated grains with micron size and a smaller share of grain boundaries, i.e. a much coarser grain structure, which results in a marked decrease in transverse impact toughness K_{CH} and material behavior characteristic for coarse grain materials, i.e. a drop in impact toughness accompanying the increase in strength.

4. Conclusions

As a result of the SPD deformation, by means of the hydrostatic extrusion process, the fragmentation of the structure to the UFG level was obtained in the AA 6060 alloy. The smallest mean grain size $d_{eq} = 291$ nm was obtained for the material with the highest true strain $\varepsilon = 2.28$. Lack of clear influence of the deformation ratio on microstructure fragmentation is caused by heat-induced dynamic healing processes during the HE process, which weaken the effects of deformation strengthening.

In the AA 6060 alloy as well as in other materials mentioned above, the HE process generates a strongly anisotropic structure characterized by the presence of equiaxed grains in the cross-section transverse to the extrusion direction and elongated grains in the form of bands in the longitudinal cross-section consistent with the extrusion direction. The structure anisotropy strongly affects the mechanical properties of the aluminum AA 6060 alloy, measured under static and dynamic conditions. Regardless of the deformation ratios, the AA 6060 alloy is characterized by weaker strength, yield strength and impact toughness in the cross-section perpendicular to the extrusion direction. The anisotropy effect of the AA 6060 alloy increases with the increase of the deformation ratio until the moment when the thermal-activated thermal softening processes weaken the strengthening effects. A particularly strong softening effect occurs at the highest plastic deformation $\varepsilon = 2.28$, in which the adiabatic temperature generated exceeds the level $T/T_m = 0.5$. The observed effect of strong structural anisotropy in the AA 6060 alloy confirms previous studies carried out on hydrostatically extruded titanium CP Ti grade 3 [27] and alloy copper CuCrZr [28], supplementing them simultaneously with the anisotropy of dynamic properties on the example of impact toughness. The material structure characteristics after the HE process and resulting from it, depending on the test direction, along with specific static and dynamic mechanical properties allow for a more effective commercial use of the AA 6060 alloy.

Acknowledgements. This work was supported in part by the National Science Centre in Poland, Project No. 2013/11/N/ST8/01976.

References

[1] J. Hirsch, "Aluminium alloy for automotive application", *Mater. Sci. Forum*. 242, 33–50 (1997).
[2] I.J. Polmear, "Light alloys: from traditional alloys to nano crystals", 4th Edition, Butterworth-Heinemann, Burlington, (2006).
[3] R.Z. Valiev, R.K. Islamgaliev, and I.V. Alexandrov, "Bulk nanostructured materials from severe plastic deformation", *Prog. Mater. Sci*. 45(2), 103–190 (2000).
[4] I.J. Beyerlein and L.S. Tóth. "Texture evolution in equal-channel angular extrusion", *Prog. Mater. Sci*. 54, 427–510 (2009).
[5] A. Vorhauer and R. Pippan, "On the homogeneity of deformation by high pressure torsion", *Scripta Mater*. 51, 921–925 (2004).
[6] P. Kral, J. Dvorak, V. Sklenicka, T. Masuda, Z. Horita, K. Kucharova, M. Kvapilova, and M. Svobodova, "Microstructure and creep behaviour of P92 steel after HPT", *Mater. Sci. Eng*. A 723, 287–295 (2018).
[7] S. Lee, Y. Saito, T. Sakai, and H. Utsunomiya, "Microstructures and mechanical properties of 6061 aluminum alloy processed by accumulative roll-bonding", *Mater. Sci. Eng*. A 325, 228–235 (2002).
[8] B. Cherukuri, T.S. Nedkova, and R. Srinivasan, "A comparison of the properties of SPD processed AA-6061 by equal-channel angular pressing, multi-axial compressions/forgings and accumulative roll bonding", *Mater. Sci. Eng*. A 410, 394–397 (2005).
[9] M. Richert, H.J. McQueen, and J. Richert, "Microband formation in cyclic extrusion compression of aluminum", *Can. Metall. Quart*. 37(5), 449–457 (1998).
[10] M. Richert, H. Petryk, and S. Stupkiewicz, "Grain refinement in AlMgSi alloy during cyclic extrusion – compression: experiment and modelling", *Arch. Metall. Mater*. 52(1), 49–54 (2007).
[11] W. Pachla, M. Kulczyk, A. Swiderska-Środa, M. Lewandowska, H. Garbacz, A. Mazur, and K.J. Kurzydłowski, "Nanostructuring of metals by hydrostatic extrusion", Proc. of 9th Int. Conf. on Metal Forming EMRS 2006, Eds. N. Juster, A. Rosochowski, Publ. House Akapit, 535–538 (2006).
[12] M. Kulczyk, S. Przybysz, J. Skiba, and W. Pachla, "Severe plastic deformation induced in Al, Al-Si, Ag and Cu by hydrostatic extrusion", *Arch. Metall. Mater*. 59, 59–64 (2014).

[13] E.O. Hall, "The deformation and ageing of mild steel: III Discussion of results", *Proc. Phys. Soc*. B 64(9), 747–753 (1951).
[14] N.J. Petch, "The cleavage strength of polycrystals", *J. Iron Steel Inst*. 174, 25–28 (1953).
[15] M. Lewandowska and K.J. Kurzydłowski, "Recent development in grain refinement by hydrostatic extrusion", *J. Mater. Sci*. 43(23), 7299–7306 (2008).
[16] L. Olejnik, M. Kulczyk, W. Pachla, and A. Rosochowski, "Hydrostatic extrusion of UFG aluminium", Int. *J. Mater. Form*. 2, 621–624 (2009).
[17] W. Pachla, M. Kulczyk, J. Smalc-Koziorowska, M. Wróblewska, J. Skiba, S. Przybysz, and M. Przybysz, "Mechanical properties and microstructure of ultrafine grained commercial purity aluminium prepared by cryo-hydrostatic extrusion", *Mater. Sci. Eng*. A 695, 178–192 (2017).
[18] M. Kulczyk, B. Zysk, M. Lewandowska, and K.J. Kurzydłowski, "Grain refinement in CuCrZr by SPD processing", *Phys. Status Solidi* A 207, 1136–1138 (2010).
[19] M. Kulczyk, J. Skiba, S. Przybysz, W. Pachla, P. Bazarnik, and M. Lewandowska, "High strength silicon bronze (C65500) obtained by hydrostatic extrusion", *Arch. Metall. Mater*. 57(3), 859–862 (2012).
[20] W. Pachla, M. Kulczyk, J. Smalc-Koziorowska, S. Przybysz, M. Wróblewska, J. Skiba, and M. Przybysz, "Enhanced strength and toughness in ultra-fine grained 99.9% copper obtained by cryo-hydrostatic extrusion", *Mater. Charact*. 141, 375–387 (2018).
[21] W. Pachla, M. Kulczyk, M. Sus-Ryszkowska, A. Mazur, and K.J. Kurzydłowski, "Nanocrystalline titanium produced by hydrostatic extrusion", *J. Mater. Proc. Tech*. 205, 173–182 (2008).
[22] W. Pachla, M. Kulczyk, S. Przybysz, J. Skiba, K. Wojciechowski, M. Przybysz, K. Topolski, A. Sobolewski, and M. Charkiewicz, "Effect of severe plastic deformation realized by hydrostatic extrusion and rotary swaging on the properties of CP Ti grade 2", *J. Mater. Process. Tech*. 221, 255–268 (2015).
[23] J. Budniak, M. Lewandowska, W. Pachla, M. Kulczyk, and K.J. Kurzydłowski, "The influence of hydrostatic extrusion on the properties of an austenitic stainless steel", *Solid State Phenomen* 114, 57–62 (2006).
[24] W. Pachla, J. Skiba, M. Kulczyk, S. Przybysz, M. Przybysz, M. Wróblewska, R. Diduszko, R. Stępniak, J. Bajorek, M. Radomski, and W. Fąfara, "Nanostructurization of 316L type austenitic stainless steels by hydrostatic extrusion", *Mater. Sci. Eng*. A 615, 116–127 (2014).
[25] M. Kulczyk, W. Pachla, A. Mazur, R. Diduszko, H. Garbacz, M. Lewandowska, W. Łojkowski, and K.J. Kurzydłowski, "Microstructure and mechanical properties of nickel deformed by hydrostatic extrusion", *Mater. Sci*. 23, 840–846 (2005).
[26] M. Kulczyk, W. Pachla, A. Mazur, M. Suś-Ryszkowska, N. Krasilnikov, and K.J. Kurzydłowski, "Producing bulk nanocrystalline materials by combined hydrostatic extrusion and equal-channel angular pressing", *Mater Sci+* 25, 991–999 (2007).
[27] E.C. Moreno-Valle, W. Pachla, M. Kulczyk, B. Savoini, M.A. Monge, C. Ballesteros, and I. Sabirov, "Anisotropy of uni-axial and bi-axial deformation behaviour of pure Titanium after hydrostatic extrusion", *Mater. Sci. Eng*. A 588, 1–7 (2013).
[28] M. Kulczyk, W. Pachla, J. Godek, J. Smalc-Koziorowska, J. Skiba, S. Przybysz, M. Wróblewska, and M. Przybysz, "Improved compromise between the electrical conductivity and hardness of the thermo-mechanically treated CuCrZr alloy", *Mater. Sci. Eng*. A 724, 45–52 (2018).
[29] W. Truszkowski and J. Kloch,"New aspects of plastic anisotropy in materials", *Bull. Pol. Ac.: Tech*. 46(3), 289–300 (1998).
[30] M. Tajally, Z. Huda, and H.H. Masjuki, "A comparative analysis of tensile and impact-toughness behavior of cold-worked and annealed 7075 aluminum alloy", *Int. J. Impact Eng*. 37(4), 425–432 (2010).
[31] P. Das, R. Jayaganthan, and I.V. Singh, "Tensile and impact-toughness behaviour of cryorolled Al 7075 alloy", *Mater. Design*. 32, 1298–1305 (2011).
[32] D.R. Fang, YZ. Tian, Q.Q. Duan, S.D. Wu, Z.F. Zhang, N.Q. Zhao, and J.J. Li, "Effects of equal channel angular pressing on the strength and toughness of Al–Cu alloys", *J. Mater. Sci*. 46, 5002–5008 (2011).
[33] K.G. Russell and M. Ashby, "Slip in aluminum crystals containing strong, plate-like particles", *Acta Metall. Mater*. 18, 891–901 (1970).
[34] M. Khadyko, S. Dumoulin, G. Cailletaud, and O.S. Hopperstad, "Latent hardening and plastic anisotropy evolution in AA 6060 aluminium alloy", *Int. J. Plasticity* 76, 51–74 (2016).
[35] T. Wejrzanowski, W.L. Spychalski, K. Różniatowski, and K.J. Kurzydłowski, "Image based analysis of complex microstructures of engineering materials", *Int. J. Appl. Math. Comp*. 18, 33–39 (2008).
[36] W. Pachla, J. Skiba, M. Kulczyk, and M. Przybysz, "High-pressure equipment for cold severe plastic deformation working of materials", *Met. Form*. XXVI(4), 283–306 (2015).
[37] W. Pachla, M. Kulczyk, A. Mazur, and M. Sus-Ryszkowska, "UFG and nanocrystalline microstructures produced by hydrostatic extrusion of multifilament wires", *Int. J. Mater. Res*. 100, (2009) 984–990 (2009).
[38] I. Alexander, S.S. Pavlov, and M. Kiritani, "Effective temperature rise during propagation of shock wave and high-speed deformation in metals", *Mater. Sci. Eng*. A 350, 245–250 (2003).
[39] F.K. Yan, G.Z. Liu, N.R. Tao, and K. Lu, "Strength and ductility of 316L austenitic stainless steel strengthened by nano-scale twin bundles", *Acta Metall. Mater*. 60, 1059–1071 (2012).